Journal Pre-proof

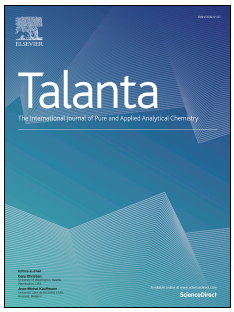

Analysis of Tau-441 protein in clinical samples using rGO/AuNP nanocomposite-supported disposable impedimetric neuro-biosensing platform: Towards Alzheimer's Disease detection

Münteha Nur Sonuç Karaboga, Mustafa Kemal Sezgintürk

PII: S0039-9140(20)30548-8

DOI: https://doi.org/10.1016/j.talanta.2020.121257

Reference: TAL 121257

To appear in: *Talanta*

Received Date: 27 March 2020

Revised Date: 29 May 2020

Accepted Date: 31 May 2020

Please cite this article as: M.N. Sonuç Karaboga, M.K. Sezgintürk, Analysis of Tau-441 protein in clinical samples using rGO/AuNP nanocomposite-supported disposable impedimetric neuro-biosensing platform: Towards Alzheimer's Disease detection, *Talanta*, https://doi.org/10.1016/j.talanta.2020.121257.

Munteha Nur SONUC KARABOGA: Conceptualization, Methodology, Visualization

Mustafa Kemal SEZGİNTÜRK: Formal Analysis, Resources, Writing – Review & Editing

GRAPHICAL ABSTRACT

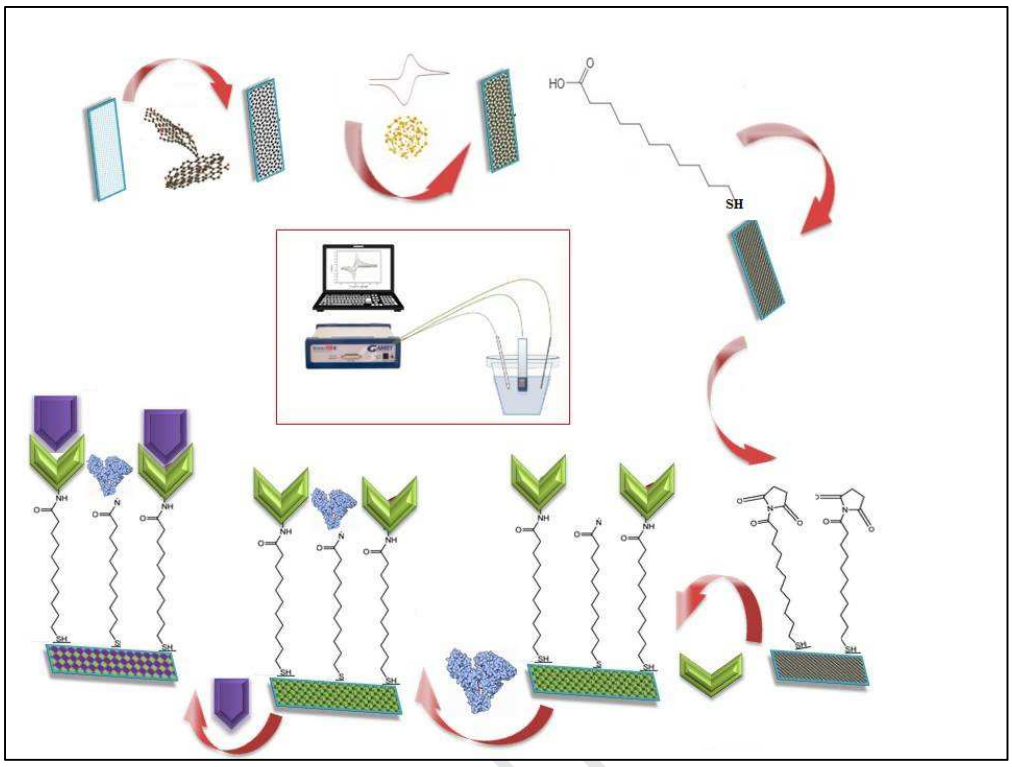

Analysis of Tau-441 protein in clinical samples using rGO/AuNP nanocomposite-supported disposable impedimetric neuro-biosensing platform: Towards Alzheimer's Disease detection

Münteha Nur Sonuç Karaboga[1] Mustafa Kemal Sezgintürk[2]

[1] Tekirdag Namik Kemal University, School of Health, Tekirdag, Turkey

[2]Canakkale Onsekiz Mart University, Faculty of Engineering, Bioengineering, Canakkale, Turkey

Correspondence: Dr Münteha Nur Sonuç Karaboga (mnsonuc@nku.edu.tr). (School of Health, 59030, Tekirdag, Turkey).

Abstract

Changes in isoforms of Tau protein, which are critical for microtubule functioning, are accepted as being responsible for diseases characterized by dementia, in particular Alzheimer's disease (AD). In this comprehensive study, a single-use neuro-biosensing probe for the determination of Tau-441 protein was developed by utilizing the power of nanocomposites consisting of reduced graphene oxide (rGO) and gold nanoparticles (AuNP) using electrochemical impedance spectroscopy (EIS) and cyclic voltammetry (CV). The nanocomposite surface (rGO-AuNP) was modified with 11-mercaptoundecanoic acid (11-MUA) act as covalent anchorer to increase the sensitivity of the assay. Surface coverage value and pinhole ratio were calculated using EIS data. Kramers-kronig data, which helps to interpret instrumental errors, are also calculated. The immunoreaction of Tau-441 with anti-Tau was monitored simultaneously with Single Frequency Impedance (SFI). The changes in surface morphology were evaluated with scanning electron microscopy (SEM), atomic force microscopy (AFM) and Fourier transform infrared spectroscopy (FTIR). The designed immunosensor showed a linear response within the concentration range of 1-500 pg / mL for the target analyte Tau-441 and the limit of detection was found to be 0.091 pg/mL. The promising point of the study is that this neuro-biosensor system can capture the Tau-441 target protein in both serum fluid and cerebrospinal fluid (CSF) samples with recoveries ranging from 96% to 108%.

Keywords: Alzheimer' disease; biosensor; electrochemical impedance spectroscopy; Tau; pinhole; reduced graphene oxide

Introduction

Alzheimer's disease (AD), the most common cause of dementia, is a chronic disease that presents as cognitive symptoms, behavioral and psychological symptoms, and thus leads to difficulty in performing daily living activities [1]. AD is characterized by the accumulation of two different proteins: senile (neuritic plaques) and neurofibrillary tangles which are associated with aggregation of microtubule protein Tau in neurons [2].

Tau is a protein that is normally found in axons and is generally unfolded to stabilize them by binding to microtubules that form the cell skeleton [3, 4]. Under pathological conditions, the phosphorylation of tau increases, which in turn reduces the affinity of the microtubules and causes imbalance in the cell skeleton, especially in neurons [5, 6]. In Alzheimer's pathology, tau and hyperphosphorylated tau are said to be among biomarkers in CSF reflecting the main pathological changes in AD. High tau levels in the CSF of patients with AD may give an idea about the neuronal injury and degeneration intensity in the brain [7, 8].

As shown in many studies, the development of neurodegenerative diseases such as Alzheimer's, Parkinson's, Huntington's disease begin approximately 10-20 years before clinical findings are seen [9-11]. For the diagnosis of AD dementia, the National Institute for the Aging-Alzheimer's Association has proposed biomarkers for investigation and as "optional clinical tools that can be used wherever and where appropriate by the clinician." The biomarker test makes the diagnosis of Alzheimer's disease more precise by contributing to evidence of the process [1, 12, 13]. The major obstacle is the inability to identify biological markers with conventional methods as their concentrations in biological fluids are low. Most of the neuro-biosensors developed for the diagnosis of biomarkers for neurodegenerative diseases promise highly sensitive, selective and impressive detection levels [14]. In this way, it contributes to diagnosis of the disease in very early stages. This urgent need for neuro-biosensors necessitates the creation of new and effective biological platforms. In this study, a nanocomposite formed with rGO and AuNP was

deposited on the surface of disposable Indium tin oxide (ITO) electrodes and a new anti-Tau-based detection probe was developed.

rGO is widely used in the biosensor field due to its large surface area provides high efficiency for antibody immobilization [15]. rGO is deposited due to high sensitivity for the determination of a wide range of analytes at various electrodes such as glassy carbon [16], indium tin oxide [15] or gold and polymers [17]. The nanomaterials act as signal-transmitting elements for the detection of chemical or biological markers and provide great promise when integrated into labels in recognition elements to mediate current flow or to indicate detection of the analyte [18]. Because the conductivity of nanostructured electrodes is extremely high, they have faster electron transfer kinetics. Nanostructured materials are highly selective due to their unique electronic structure and the surface chemistry of these materials can be adjusted to the type of analyte [19, 20]. AuNPs are inert, and can be easily modified for the target analyte. They can react with molecules containing various functional groups, such as thiols or amines, and allow these functional groups to be biologically functionalized with different ligands (peptides, proteins and aptamers) in order to specifically identify biological targets [21]. While the antibodies immobilize to the surface by self assembly, reducing the binding capacity of the target antigen, immobilization to a gold-modified surface contributes positively to many analytical characteristics, especially the selectivity of antigens [22].

The resulting nanocomposite with rGO-AuNP offers high efficiency for the immobilization of the antibody and selective determination of the Tau-441 protein. In addition to extensive analytical evaluations, the aim of the study is to evaluate the sensing ability of the developed system in CSF and serum.

Materials and Methods

Reagents and apparatus

The characteristics of ITO-coated PET (polyethyetheraphthalate) films used as working electrodes are as follows: conductivity and surface resistance 550 nm (> 79%) and 60 Ω -

respectively and electrode dimensions of 2 × 0.5 cm. (Supply Company: Sigma-Aldrich, St. Louis, MO, USA). Ag/AgCl reference electrode was saturated with KCl and counter (platinum wire) (Supply Company: iBAS, Warwickshire, UK). Tau-441 from human plasma and monoclonal anti-Tau antibody from rabbits were obtained from Sigma Aldrich (St. Louis, MO, USA). Tau-441 and anti-Tau stock solutions were maintained at -20 °C at certain concentrations until studies were performed. Gold (III) chloride trihydrate was obtained from Sigma Aldrich (St. Louis, MO, USA) and rGO was supplied from Graphene Supermarket (Graphene Laboratories, Inc. 4603 Middle Country Rd. Unit 125 Calverton).

1 M KCl containing 5 mM $[Fe(CN)6]^{4-}$ and 5 mM $[Fe(CN)6]^{3-}$ was prepared in 50 mM phosphate buffer for use as a redox probe.

FTIR spectra, AFM and SEM analyzes operating in the range of 4000-400 cm^{-1}, were recorded in order to investigate the nature of the bonds on the surface when developing the neuro-biosensor. Morphological changes in nanocomposites and immobilization steps were monitored by SEM (FEI-Quanta FEG 250 Model) and AFM. AFM analysis was performed at NKÜ Scientific and Technological Research Center (NABILTEM) using AFM PLUS +, NanoMagnetic Instruments. Images were obtained using the AFM tapping mode (256 x 256 points with scan rate 5µm/s.).

Preparation of electrodes and modification with rGO

Before proceeding to the advanced design steps of the neuro-biosensor, the ITO-PET disposable electrodes are cleaned as described in our previous study in detail [23]. rGO solution dispersed in dimethylformamide [24] was prepared by sonication for 60 minutes with ultrasound. Then, 15 µL of the prepared rGO dispersion solution was dropped onto clean ITO-PET electrodes and the electrodes were allowed to dry overnight.

Design methodology for Tau-441 neuro-biosensing platform

The ITO electrodes modified with rGO were dipped in an electrochemical cell containing $HAuCl_4.3H_2O$ (1 mM) solution prepared in 50 mM pH 7.0 phosphate buffer. Electrochemical

deposition of gold nanoparticles onto the ITO surface was carried out with 10 consecutive cycles at a scanning rate of 50 mV/s between -0.2 V- (-) 1.3 V potential [25]. The resulting ITO electrodes with rGO-AuNP nanocomposite were washed with ultra-pure water and then dried with ultra-pure argon gas. The ITO electrodes rGO-AuNP nanocomposite formed on the surface were immersed into 11-MUA solution prepared in ethanol and allowed to incubate overnight. After incubation, the electrodes were first washed with ethanol, then washed with ultra-pure water. The nanocomposite-doped 11-MUA-modified electrodes were incubated for 60 minutes at room temperature by immersion in an aqueous solution containing 0.4 mM N-(3-Dimethylaminopropyl)-N-ethylcarbodiimide hydrochloride (EDC) and 0.1 mM N-hydroxysuccinimide (NHS) for activation of the carboxylic acid terminal groups found in 11-MUA and their covalent interaction with the amino groups in the anti-Tau antibody. The electrodes were washed with ultra-pure water and dried with ultra-argon gas, then immersed in solutions containing 100 µL of anti-Tau and incubated for 60 minutes at room temperature in a dark environment. After incubation with the anti-Tau antibody, the electrodes were washed with ultrapure water to remove unbound antibody molecules and then dried with argon gas. Finally, the antibody-immobilized electrodes were incubated for 60 minutes in 0.5% BSA solution to block non-reactive ends and prevent non-specific interactions. After this last step, the neuro-sensor prepared was maintained at + 4 °C until Tau-441 measurements were performed.

Scheme 1

Determination of Tau-441 with the neuro-biosensing platform

Each of the 11-MUA-modified ITO-based electrodes with nanocomposite added (rGO-AuNP) were incubated for 60 minutes at room temperature in the dark with standard Tau-441 solutions prepared at different concentrations. After the incubation period, the neuro-biosensor was gently washed in ultra-pure water to remove physically-adsorbed Tau-441 molecules. EIS and CV measurements for each Tau-441 concentration were performed by measurements at the working

electrodes in the redox solution. EIS and CV measurements were recorded with EChem Analyst software program.

CSF and serum samples analysis

The amount of Tau-441 in human cerebrospinal fluid and human serum was analyzed using the standard addition method to evaluate the usefulness of the nanocomposite-doped neuro-biosensor system in clinical applications. Tau-441 concentrations used for standard addition were 100 pg/mL and 400 pg/mL. Measurements were repeated 3 times for each CSF and serum sample. The CSF and serum samples were randomly selected from Namik Kemal University Medical Faculty 2013/86/07/05 with the approval of the ethics committee. CSF and serum samples were stored in specific portions at -20 °C until measurements were performed.

Results and Discussion

Evaluation of fabrication steps for neuro biosensing platform by EIS and CV

A synergistic cooperative-based hybridizing biosensor between rGO and AuNPs was developed to enhance electrochemical performance for determination of the Tau-441 protein. The nanocomposite formed by rGO-AuNP was left in the 11-MUA solution overnight and was expected to form strong covalent interactions with SH on the surface to form SAMs. SAMs not only cover the surface but also reduce the number of random orientations and produce smooth, reproducible and stable structures [26].

Figure 1 clearly shows the cyclic voltammograms recorded during the electrochemical synthesis of Au nanoparticles by electrochemical deposition on the ITO surface modified with rGO.

Figure 1

The prominent peak in Figure 1, which indicates the difference in the surface. In addition, reduction of Au in the first cycle occurred at about -960 mV against the Ag/AgCl reference electrode, but the reduction potential with the repeated screening cycles shifted to -1.020 V

(small graph inserted in Figure 1) due to nucleation on the accumulation. This shift is indicative of the accumulation of gold nanoparticles on the surface.

ITO electrodes with rGO-AuNP nanocomposite were allowed to incubate overnight in 11-MUA solution. Formation of the SAMs layer and covalent interaction occurred between the Au surface and -SH, while the functional -COO terminals were treated with EDC and NHS to ensure efficacy in the immobilization of anti-Tau. The cross-linking of the EDC-NHS with the anti-Tau on the carboxylic acid groups of 11-MUA resulted in the immobilization of anti-Tau on the surface.

In the impedance spectra of the steps involved in the construction of the neuro-biosensor for determination of Tau-441, the charge transfer changes for each step and the voltammograms from the CV are shown in Figure 2.

Figure 2

EIS provides detailed information about the change in the surface properties of modified electrodes. The semicircular diameter at high frequencies corresponds to the Rct while the linear part at low frequencies corresponds to the diffusion process. Figure 2.A and Figure 2.B show that the bare ITO electrode has a very high charge transfer resistance (approx. 20×2=40 kohm) due to its insulating properties. However, after the rGO-AuNP nanocomposite was deposited on the ITO, a smaller Rct was observed (Supporting information). Since rGO - AuNPs composites are excellent electrically conductive materials, they accelerate the transfer of electrons causing Rct to fall. SAMs, which occur on the surface after interaction between -SH groups of 11-MUA and the nanocomposite modified surface, caused an increase in charge transfer resistance due to functional COO-terminals pushing the redox probe and making diffusion difficult. As a result of the covalent immobilization of the anti-Tau protein on the surface, the insulating layer formed by the protein layer prevents the transfer of electrons at the interface, which is reflected as a significant increase in charge transfer resistance (about 10 kohm).

The heterogeneous electron transfer rate constant value (k0) of the redox probe is a distinctive element used to verify the electronic transport process in the nanocomposite film. According to the charge transfer kinetics, k0 is expressed as follows [27]:

$$k^0=RT/n_1^2F^2AR_{ct}C \quad (1)$$

where R is the gas constant, T is temperature, n is the number of electrons involved in the electrode reaction, F is the Faraday constant, A is the electrode area (0.25 cm^2) and C is the concentration of the redox probe.

Table 1 shows the changes in the resistance and capacitance of the neuro-biosensor system together with the k^0 values. The rGO film on the ITO electrode surface after the accumulation of gold nanoparticles showed a very high k^0 value, a result of increased electron transport. Subsequently, the immobilization of anti-Tau caused a significant decrease in the value of k^0 (2.12×10^{-7} m s^{-1}); this confirms the slow transport of electrons due to the insulating property of the protein molecules and the formation of the bioelectrode.

The progressive steps in the neuro-biosensor system consisting of rGO and AuNP nanocomposite and ultimately the immobilization of the anti-Tau on the sensing surface increased the double charge layer thickness and inhibited the interface electrochemical process of the redox probe. Electrode capacitance, Cdl, decreases and electron transfer resistance, Rct, increases. This is the result of impedimetric behavior of the neuro-biosensor system.

Table 1

The development steps for the neuro-biosensor system were also followed by CV (Figure 2C). When developing the neuro-biosensor system for the determination of Tau-441, the peak potential separation between anodic and cathodic waves ($\Delta E_p = E_{pc} - E_{pa}$) was 0.32 V at the ITO electrode modified with rGO and increased to 0.46 V after the gold nanoparticles were deposited. After the SAMs were generated with 11-MUA on the modified ITO surface with rGO-AuNP nanocomposite, the ΔE_p value increased rapidly to 1.02 V. This is used for the electrochemical evaluation of the conductivity of the electrode and is inversely proportional to

the electron transfer rate. This rapid increase is evidence that in addition to the aliphatic groups of the 11-MUA, the conductivity is greatly reduced due to the carboxylic terminals.

Modification of the electrode surfaces with a resistant monolayer results in passivation, and thus changes the alternating current (ac) responses. In terms of the equivalent circuit, two components will be affected. At higher frequencies where the electrode reaction is fully kinetic-controlled, heterogeneous charge transfer resistance is expected to increase due to the inhibition of the electron transfer rate. At low frequencies, the Warburg impedance is expected to deviate from the linear dependence to $\omega^{-1/2}$. This deviation occurs when the defects or pinholes in the single layer are very different from the diffusion layer thickness. However, when the diffusion layers overlap with the pinholes, the ac response at low frequencies is similar to the behavior of the bare electrodes [28-30].

The surface coverage value ($\boldsymbol{\theta}_{\mathbf{EIS}}$) can be determined from the following equation (2) after forming SAM with 11-MUA on the nanocomposite-modified ITO surface:

$$\boldsymbol{\theta}_{\mathbf{EIS}} = 1 - \left(\frac{Rct^{AuNP}}{Rct^{SAMs}}\right) \qquad (2)$$

Rct^{AuNP} is the charge transfer resistance of the gold nanoparticles deposition step, and Rct^{SAMs} is the charge transfer resistance of the mono layer formation on the gold nanoparticle-coated electrode surface. In the light of these data, the value of $\boldsymbol{\theta}_{\mathbf{EIS}}$ was 0.975. However, Amatore et al. [30] suggest that when the $\boldsymbol{\theta}_{\mathbf{EIS}}$ value reaches $\boldsymbol{\theta}_{\mathbf{EIS}} > 0.9$, it is not sufficient to find equation 2. In this case, the surface coverage value can be estimated using a pattern based on the pinhole size [30] :

$$\boldsymbol{\theta}_{\mathbf{EIS}} = 1 - \left(\frac{\sigma_W}{m - \sigma_W}\right) \qquad (3)$$

$\boldsymbol{\theta}$w is the Warburg coefficient and this coefficient is calculated using the Yo value obtained from the equivalent circuit model of the AuNP-coated electrode using the following equation:

$$\sigma = {}^{1}/_{Yo.\sqrt{2}} \quad (4)$$

The value of m is the slope of the linear range observed in the high frequency region of the graph Z ′ vs $\omega^{-1/2}$ obtained from the electrode modified with 11-MUA. According to equation 3, θ_{EIS} was found to be 0.9925.

The radius of the defects in the single layer and the distance between them were estimated using the microarray model proposed by Amatore et al. [31] According to this model, it is assumed that pinholes are active regions with a uniform radius and are distributed uniformly in a single layer [32].

The cross-section of the pinhole area (1- $\boldsymbol{\theta}_{\mathbf{EIS}}$) may be related to the size of the pinholes and the distance between adjacent pinholes:

$$\left(\mathbf{1}\text{-}\boldsymbol{\theta}_{\mathbf{EIS}}\right)= \frac{\mathbf{ra^2}}{\mathbf{rb^2}} \quad (5)$$

Where ra is the radius of the pinhole and rb is the radius of the non-active area surrounding the electrode. The pinhole radius can be determined from the frequency value corresponding to the pivot point between the high and low frequency field in Z ″ - $\omega^{-½}$, and this frequency value is easily calculated from the maximum of the Z ″ - $\omega^{-½}$. Tokuda et al. [33] expressed this maximum frequency with equation 6:

$$\omega= \frac{q}{2} \quad (6)$$

where q is the radial frequency of the transition. Supporting information Figure 1S is the Z″ - $\omega^{-½}$ graph of the 11-MUA-modified electrode and the maximum frequency from the graph is seen to be 7.97 Hz. In this case ra and rb can be calculated from the following equation:

$$q=\frac{D}{0{,}36\ ra^2} \tag{7}$$

D is the diffusion coefficient of the redox species and is 7.6×10^{-6} cm^2 s^{-1} [34].

$$1\text{-}\boldsymbol{\theta}_{\mathbf{EIS}}=\left(\frac{\sigma_W}{m\text{-}\sigma_W}\right)=\frac{ra^2}{rb^2} \tag{8}$$

According to these equations, the pinhole radius (ra) of 11-MUA SAM is calculated as 1.1 µm, while the centers of two adjacent pinholes (rb) are at a distance of 12.7 µm. For many SAM-coated electrodes, these values are expected to be in the range of 0.1-10 µm and 1-100 µm, respectively, so the results are consistent with previous studies [30, 35, 36].

Optimization parameters of Tau-441 neuro-biosensor

The optimization parameters required for the reproducible neuro-biosensing system were tested. The experimental details of the optimization studies (effect of rGO concentration, optimum 11-MUA concentration, optimum anti-Tau concentration) and the obtained results are given in the supporting information (Figure 2S, 3S)

Analytical properties of the developed neuro-biosensor system

Standard Tau-441 solutions prepared with different concentrations and the neuro-biosensor system with optimum conditions were measured by EIS and CV techniques. The relationship between the Tau-441 concentration and the electron transfer resistance was determined by the equivalent circuit model added to Figure 2.A.

In the case of very rapid electron transfer processes on the biosensor surface, the linear portion of the impedance spectrum along with the radius portion is also located in the Nyquist graph,

but a very slow electron transfer step results in a large semicircular region without a linear part, as seen in Figure 3.A. The calibration graph of the Tau-441 neuro-biosensor was plotted using the following equation.

$$\Delta Rct = Rct(Tau\text{-}441) - Rct(BSA)$$

The concentration-dependent increase in Rct is indicative of the formation of an antigen-antibody complex with immunoreaction; and this creates a kinetic barrier that disrupts interfacial electron transport at the bioelectrode surface. The calibration plot (Figure 3.B) drawn with data from the EIS spectrum showed that the developed neuro-biosensor system gave a linear correlation in the range of 1-500 pg/mL (Figure 3.B). The values of LOD (detection limit) and LOQ (quantitative limit) for Tau-441 were determined as 0.091 pg/mL and 0.3 pg/mL, respectively, for the nanocomposite-modified neuro-biosensor system. These results emphasize that the AuNP-rGO hybrid structure has excellent capture ability for Tau-441 antibody-antigen binding.

Figure 3

The capacitance of the electrochemical double layer (Cdl) depends on the solvent molecules, the immobilized biomolecules, the films supporting the immobilization and detection processes, and all the compounds present at the interface. When the dielectric constant or the thickness of the double layer on the transducer surface changes, a capacitance change is induced [37]. When forming a capacitive biosensor, the electrode surface is usually covered with an additional insulating layer to reduce faradaic currents (i.e. to increase the charge transfer resistance in parallel with the capacitance). The biological detection element is immobilized on this layer. While increasing the capacitance with increasing Tau-441 concentration, charge transfer resistance increases (Table 1). This is the impedimetric proof that increasing concentrations of Tau-441 (1-500 pg/mL) can be measured with the developed biosensing platform.

The results of the cyclic voltammograms for Tau-441 biomarker in the concentration range of 1-500 pg/mL are shown in Figure 3.C. The anodic and cathodic peak currents decreased due to increasing Tau-441 concentration. This is the manifestation of the barrier resistance on the surface to the electrons with increasing protein concentration which have difficulty in diffusing to the surface. At this point, we can state that the CV and EIS results comply with each other.

The values of Kramers Kronig transformations (K.K.T) of the neuro-biosensor system developed for the determination of Tau-441 are given in Table 1. In principle, K.K.T are used to determine whether the impedance spectrum of the system is affected by, for example, bias caused by instrumentation or time-dependent phenomena. K.K. transformations can be evaluated to show that the equivalent circuit model is insufficient. [38-40]. The K.K transform values of the rGO-AuNP-based neuro-biosensor emphasize that the data for impedance obtained from the developed system and the data presented by the equivalent circuit model are in harmony. As the development steps of the sensor progressed, a more linear and stable K.K conversion was observed.

Repeatability of measurements using a biosensor system mean that the measurements are made by the same instrument and method, where human input is required the same observer participates and the measurements are made for a short period of time when the basic value can be considered to be constant. The repeatability of the ITO-based rGO-AuNP nanocomposite-modified and 11-MUA-doped neuro-biosensor was determined by analyzing the same concentration of Tau-441 (100 pg/mL) prepared with 20 single-use electrodes under optimum conditions. As a result of repeatability studies, the coefficient of variation, mean value and standard deviation of the system were calculated as 6.38%, 105.95 and 6.70 pg/mL, respectively.

The reproducibility of the neuro-biosensor for Tau-441 assay was assessed by monitoring the Tau-441 responses in the range of 1-500 pg/mL of the 6 biosensor systems prepared at different

times with the same procedure. As a result of the reproducibility studies, it was found that the responses of 6 neuro-biosensors showed similar linearity for Tau-441 and 1-500 pg/mL. The relative standard deviations of the slopes and intercepts of the reproducibility shown in Figure 4S were found to be 3.02% and 3.41%, respectively. The main point in reproducibility studies is that the biorecognition element is immobilized on the sensor surface by preserving the biological activities and thus repeated measurements can be made.

The interaction between receptor-ligand and the strength of this interaction in an immunosensor directly affects the reusability and analytical responses of the immunosensor. When the lifetime of the receptor ligand complex is too long, its regeneration capacity also increases. Therefore, the evaluation of the lifetime of the complex is very important especially in biosensor studies developed for biomedical purpose [41]. The regeneration of the developed neuro-biosensor was performed by immersing the sensing electrodes in 0.05 M pH 3.5 glycine-HCl buffer for 5 minutes to dissociate the Tau-441 antibody-antigen immuno-complex. While the electrodes gave approximately the same impedimetric response to the concentration of 100 pg/mL of Tau-441 over 4 cycles, rGO material began to pour from the electrode surface after the 4th cycle.

Selectivity is the ability of the biosensor to perceive the target molecule from within the analytical environment. Figure 3.B shows that HSP-70, SYN alpha and RACK-1 make a very small contribution to the biosensor. This insignificant contribution for nonspecific interactions of some proteins to the total Rct response is the result of the high selectivity of the biosensor against the specific target Tau-441. The ability of a biosensor to distinguish a target analyte from other species in a complex matrix is key to successful applications in real-time monitoring. Although the formation of the immunocomplex can be selective, the signal transduction process is usually prevented by the presence of other undesired substances and their effects on the electron transfer path. In this regard, it is thought that modifying the sensing surface with rGO-AuNP nanocomposite doping and with 11-MUA contributes to the selectivity of the system.

Stability is the ability to produce a signal of the same magnitude when a biosensor is repeatedly used with the same analyte concentration over time. It can also be evaluated by monitoring the sensor sensitivity intermittently during a given storage period. The ability of the neuro-biosensor system to measure the same concentration (100 pg/mL) of Tau-441 was monitored for 10 weeks (Figure 5S supporting information). It was observed that the system maintained its stability for 8 weeks and a partial reduction in the impedance signal occurred from 9th week onwards. This emphasizes that the neuro-biosensor system developed has an effective storage capacity. However, decreases in the signal may be related to the loss of adsorption force over time and thus deterioration of the sensing unit.

Single frequency impedance

The kinetic behavior of the immunocomplex between Anti-Tau and Tau-441 was evaluated by monitoring the changes in impedance and phase angle at constant frequency in a non-faradaic environment. The selection and analysis of the frequency (10 Hz) to be applied to the system were determined with the help of the Bode curve. Figure 4A shows the Bode plot for the neuro-biosensor. Bode graphics provide information about the kinetics at the electrode/solution interface for various applied frequencies. The rGO-modified electrode showed capacitive properties at a frequency range of 10 to 3,000 Hz, and a frequency of <10 Hz. It then shifted to the frequency range seen in Figure 4 by the immobilization of anti-Tau, which is an indication of immobilization.

Figure 4

The impedimetric follow-up at 10 Hz for the formation of the immunocomplex between Anti-Tau and Tau-441 is as shown in Figure 4B. The formation of the immunocomplex is completed in about 2000 s seconds (35 minutes). At the end of this period, while the change in impedance is about 250 ohms, the change in the phase angle is 4°. SFI data are evidence that Tau-441 successfully interacts with the biosensing platform. SFI analysis is an EIS technique used to

reduce the complexity of a single frequency, signal acquisition and processing, making it a convenient, simple and inexpensive analysis technique. Thus, the sensor provides advantages such as rapid response, low cost and high analysis power for clinical experiments.

Evaluation of Tau-441 level in clinical samples

The amount of Tau-441 found in CSF and serum samples collected randomly from patients who attended Namik Kemal University neurology clinic was determined by the present neuro-biosensor system. To assess the analytical reliability of the produced neuro-biosensor, Tau-441 was analyzed using the standard addition method in human cerebrospinal and serum fluid. There are studies showing that the average value of Tau in healthy men and women in CSF is 250 pg/mL [42] and the mean value in serum is 15 pg/mL [43]. The results obtained with the developed neuro-biosensor system using the standard addition method are shown in Table 2. When the chart is examined, it is seen that the neuro-biosensor system developed more sensitive responses in the CSF environment. When the statistical results are evaluated together, it can be stated that rGO-AuNP nanocomposite-11-MUA-modified neuro-biosensor system is promising for clinical use in detection of Tau-441, an Alzheimer's biomarker.

Table 2

SEM, AFM and FTIR results

Morphological changes in the neuro-biosensor system during the step-by-step development were visualized by scanning electron microscopy (Figure 5). Figure 5A shows the adsorption of rGO on the bare ITO surface. The freckled image formed after the deposition of gold nanoparticles on the surface modified with rGO indicates the nanoparticles (5B). When the rGO-AuNP composite structure was treated with 11-MUA, the formation on the surface changed again to form 5C. The surface after the anti-Tau immobilization on the structure is clearly visible with globular form in Figure 5D. In the step where BSA was immobilized on the

surface in order to prevent non-specific adsorption, the morphology of the surface was transformed into Figure 5E. As a result of the immuno-interaction of Tau-441 with the bio-recognition unit, the morphology of the surface has a branched appearance as seen in Figure 5F.

Figure 5

The surface morphology of the neuro-biosensor system for the determination of Tau-441 was also evaluated with AFM (Figure 7S). Changes in the surface roughness of the Tau-441 neuro-biosensor were evaluated by root mean square (rms). RMS roughness is the square root of the distribution of surface height and is considered to be more sensitive than the average roughness in cases where there are large deviations from the mean. It represents the standard deviation of the surface profile changes and is used in computations of skew and kurtosis [43]. While the RMS value for the step where the surface was conductive with rGO was 0.54 µm, it was 0.48 µm after the gold nanoparticles were deposited on the surface. With the immobilization of Anti-Tau, the formation of an insulating layer on the surface was reflected as 0.32 µm. In the last step, as a result of the interaction of the Tau-441 with the biorecognition unit, the RMS value was 0.29 µm. All these data and AFM images support the formation of neuro-biosensors on the surface.

Comparison of the designed Tau-441 neuro-biosensor with previously-reported studies is shown in the table. There are many studies reporting that the amount of this protein in body fluids may be important in the early diagnosis of disease. However, the electrochemical-based biosensor systems for Tau determination in the literature are quite limited. The detection platform used in the design of the biosensor allowed Tau-441 to be determined at 0.091 pg/mL This value is relatively remarkable to other studies, considering the practicality and cost of the developed system. In addition, the neuro-biosensor system developed was proven to have clinical applicability potential by analyzing the amount of Tau-441 found in both serum and CSF. This study, which is quite valuable in this respect, is promising.

Table 3

Conclusions

The aggregation of Tau protein and the formation of tangles in AD are among the key points in the disease. Early detection of this protein may have a significant effect on the course of the disease and the quality of life of the patient. Thanks to the nanocomposite platform consisting of gold nanoparticles and rGO, this biomarker was identified in a selective, sensitive and wide range (1-500 pg/mL). In addition, the neuro-biosensor platform has high reproducible, repeatable and storage capability. The single-use electrode (ITO) used in the production of the developed biosensing platform increases the practicality of the study. ITO-PET electrodes are open to modifications but have low cost. The highlight of the study is that the rGO-AuNP-based 11-MUA-modified neuro-biosensor platform can analyze the Tau-441 protein in both CSF and serum selectively. On the other hand, the handicap of the study is that it takes a long time to prepare the sensing probe (about 2 days when incubations are included). Sensing probe can be prepared faster and time can be saved if practical solutions are offered to shorten incubation times with further studies. Also, working with a larger number of real samples can make it possible to test the reliability of the developed neuro-biosensing probe.

References

[1] A. Nahar, A. Lukose, R.G. Ramesh, S. Purokayastha, S.H. Kadiveti, et al, Alzheimer's Dementia: An Overview, J Indian I Sci. 97 (2017) 591-602. https://doi.org/10.1007/s41745-017-0051-3.

[2] L.M. Shaw, M. Korecka, C.M. Clark, V.M-Y. Lee, J.Q. Trojanowski, Biomarkers of neurodegeneration for diagnosis and monitoring therapeutics, Nat. Rev. Drug Discov 6 (2007) 295-303. https://doi.org/10.1038/nrd2176.

[3] M.G. Spillantini, and M. Goedert, Tau pathology and neurodegeneration, Lancet Neurol. 12 (2013) 609-622. https://doi.org/10.1016/S1474-4422(13)70090-5

[4] M. Dani, D. Brooks and P. Edison, Tau imaging in neurodegenerative diseases, Eur J Nucl Med Mol Imaging. 43 (2016) 1139-1150. https://doi.org/10.1007/s00259-015-3231-2

[5] T. Guo, W. Noble, and D.P. Hanger, Roles of tau protein in health and disease, Acta Neuropathol. 133 (2017) 665-704. https://doi.org/10.1007/s00401-017-1707-9

[6] A.W. Fitzpatrick, B. Falcon, S. He, A.G. Murzin, G. Murshudov, et al, Cryo-EM structures of tau filaments from Alzheimer's disease, Nature 547 (2017):185-190. https://doi.org/10.1038/nature23002

[7] I. Gozes, G. Höglinger, J.P. Quinn, N.M. Hooper, and K. Höglund Tau diagnostics and clinical studies, J Mol Neurosci. 63 (2017) 123-30. https://doi.org/10.1007/s12031-017-0983-0

[8] C. Rosén, O. Hansson, K. Blennow, H. Zetterberg Fluid biomarkers in Alzheimer's disease–current concepts, Mol Neurodegener. 8 (2013) 20. https://doi.org/10.1186/1750-1326-8-20

[9] D.E. Bredesen Neurodegeneration in Alzheimer's disease: caspases and synaptic element interdependence, Mol Neurodegener. 4 (2009) 27. https://doi.org/10.1186/1750-1326-4-27

[10] K.S. Sheinerman, and S.R. Umansky, Circulating cell-free microRNA as biomarkers for screening, diagnosis and monitoring of neurodegenerative diseases and other neurologic pathologies, Front Cell Neurosci. 7 (2013) 150. https://doi.org/10.3389/fncel.2013.00150

[11] M. Gómez-Río, M.M. Caballero, J.M. Górriz Sáez, , and A. Mínguez-Castellanos, Diagnosis of neurodegenerative diseases: the clinical approach, Curr. Alzheimer Res, 13 (2016) 469-474. https://doi.org/10.2174/1567205013666151116141603

[12] N. Sheikh-Bahaei, S.A. Sajjadi, and A.L. Pierce, Current Role for Biomarkers in Clinical Diagnosis of Alzheimer Disease and Frontotemporal Dementia, Curr Treat Options Neurol. 19 (2017) 46. https://doi.org/10.1007/s11940-017-0484-z

[13] G.M. McKhann, D.S. Knopman, H. Chertkow, B.T. Hyman, Jr C.R. Jack, et al, The diagnosis of dementia due to Alzheimer's disease: Recommendations from the National Institute on Aging-Alzheimer's Association workgroups on diagnostic guidelines for Alzheimer's disease, Alzheimers Dement. 7 (2011) 263-269. https://doi.org/10.1016/j.jalz.2011.03.005

[14] K.M. Bell, and S.E. Kornguth, Biosensors for Neurological Disease, in: Marks, R. (Ed), Handbook of Biosensors and Biochips. John Wiley & Sons (2008) https://doi.org/10.1002/9780470061565.hbb139

[15] A. Benvidi, N. Rajabzadeh, M. Mazloum-Ardakani, M.M. Heidari, and A. Mulchandani, Simple and label-free electrochemical impedance Amelogenin gene hybridization biosensing based on reduced graphene oxide. Biosens. Bioelectron. 58 (2014) 145-152. https://doi.org/10.1016/j.bios.2014.01.053

[16] A. Benvidi, A. Dehghani-Firouzabadi, M. Mazloum-Ardakani, B-B.F. Mirjalili, R. Zare, Electrochemical deposition of gold nanoparticles on reduced graphene oxide modified glassy carbon electrode for simultaneous determination of levodopa, uric acid and folic acid, J. Electroanal. Chem. 736 (2015) 22-29. https://doi.org/10.1016/j.jelechem.2014.10.020

[17] R.K. Layek, and A.K. Nandi, A review on synthesis and properties of polymer functionalized graphene, Polymer 54 (2013):5087-103. https://doi.org/10.1016/j.polymer.2013.06.027

[18] W. Zhang, Z. Guo, Y. Chen, and Y. Cao, Nanomaterial based biosensors for detection of biomarkers of exposure to OP pesticides and nerve agents: a review, Electroanal. 29 (2017) 1206-12013. https://doi.org/10.1002/elan.201600748

[19] B.J. Sanghavi, S. Sitaula, M.H. Griep, S.P. Karna, M.F. Ali et al, Real-time electrochemical monitoring of adenosine triphosphate in the picomolar to micromolar range using graphene-modified electrodes, Anal chem. 85 (2013) 8158-8165. https://doi.org/10.1021/ac4011205

[20] B.J. Sanghavi, O.S. Wolfbeis, T. Hirsch, N.S. Swami, Nanomaterial-based electrochemical sensing of neurological drugs and neurotransmitters, Mikrochim Acta. 182 (2015) 1-41. https://doi.org/10.1007/s00604-014-1308-4

[21] M. Varna, H.V. Xuan, E. Fort, Gold nanoparticles in cardiovascular imaging (2018). Wiley Interdiscip Rev Nanomed Nanobiotechnol 10:e1470. https://doi.org/10.1002/wnan.1470

[22] J. Baniukevic, İ.H. Boyaci, A.G. Bozkurt, U. Tamer, A. Ramanavicius, A. Ramanaviciene, Magnetic gold nanoparticles in SERS-based sandwich immunoassay for antigen detection by well oriented antibodies, Biosens Bioelectron. 43 (2013) 281-288. https://doi.org/10.1016/j.bios.2012.12.014

[23] M.N. Sonuç Karaboğa, M.K. Sezgintürk, Cerebrospinal fluid levels of alpha-synuclein measured using a poly-glutamic acid-modified gold nanoparticle-doped disposable neuro-biosensor system, Analyst. 144 (2019) 611-621. https://doi.org/10.1039/c8an01279b

[24] J. Paredes, S. Villar-Rodil, A. Martínez-Alonso, J. Tascon, Graphene oxide dispersions in organic solvents, Langmuir 24 (2008) 10560-10564. https://doi.org/10.1021/la801744a

[25] Y. Ma, J. Di, X. Yan, M. Zhao, Z. Lu, Direct electrodeposition of gold nanoparticles on indium tin oxide surface and its application, Biosens Bioelectron. 24 (2009) 1480-1483. https://doi.org/10.1016/j.bios.2008.10.007

[26] E. Katz, and I. Willner, Probing biomolecular interactions at conductive and semiconductive surfaces by impedance spectroscopy: routes to impedimetric immunosensors,

DNA sensors, and enzyme biosensors, Electroanal. 15 (2003) 913-947. https://doi.org/10.1002/elan.200390114

[27] N. Puri, A. Niazi, A.K. Srivastava, Synthesis and Characterization of Reduced Graphene Oxide Supported Gold Nanoparticles-Poly (Pyrrole-Co-Pyrrolepropylic Acid) Nanocomposite-Based Electrochemical Biosensor, Appl Biochem Biotechnol. 174 (2014) 911-925. https://doi.org/10.1007/s12010-014-0997-9

[28] C. Cannes, F. Kanoufi, and A.J. Bard, Cyclic voltammetry and scanning electrochemical microscopy of ferrocenemethanol at monolayer and bilayer-modified gold electrodes, J Electroanal Chemistry. 547 (2003) 83-91. https://doi.org/10.1016/S0022-0728(03)00192-X

[29] F.G. Chevallier, L. Jiang, T.G. Jones, R.G. Compton, Mathematical modelling and numerical simulation of cyclic voltammetry at an electrode covered with an insulating film containing cylindrical micropores, J Electroanal Chem. 587 (2006) 254-262. https://doi.org/10.1016/j.jelechem.2005.11.016

[30] D. García-Raya, R. Madueño, J.M. Sevilla, M. Blázquez, T. Pineda, Electrochemical characterization of a 1, 8-octanedithiol self-assembled monolayer (ODT-SAM) on a Au (1 1 1) single crystal electrode, Electrochim Acta. 53 (2008) 8026-8033. https://doi.org/10.1016/j.electacta.2008.06.017

[31] C. Amatore, J.M. Savéant., and D. Tessier, Charge transfer at partially blocked surfaces: a model for the case of microscopic active and inactive sites, J Electroanal Chem Interfacial Electrochem. 147 (1983) 39-51. https://doi.org/10.1016/S0022-0728(83)80055-2

[32] P. Diao, M. Guo, and R. Tong, Characterization of defects in the formation process of self-assembled thiol monolayers by electrochemical impedance spectroscopy, J Electroanal Chem. 495 (2001) 98-105. https://doi.org/10.1016/S0022-0728(00)00424-1

[33] K. Tokuda, T. Gueshi, and H. Matsuda, Voltammetry at partially covered electrodes: Part III. faradaic impedance measurements at model electrodes, J Electroanal Chem Interfacial Electrochem. 102 (1979) 41-48. https://doi.org/10.1016/S0022-0728(79)80027-3

[34] J. Gooding, V. Praig, and E. Hall, Platinum-catalyzed enzyme electrodes immobilized on gold using self-assembled layers, Anal Chem. 70 (1998) 2396-2402. https://doi.org/10.1021/ac971035t

[35] S. Campuzano, M. Pedrero, C. Montemayor, E. Fatás, J.M. Pingarrón, Characterization of alkanethiol-self-assembled monolayers-modified gold electrodes by electrochemical impedance spectroscopy, J Electroanal Chem. 586 (2006) 112-121. https://doi.org/10.1016/j.jelechem.2005.09.007

[36] H.O. Finklea, L. Liu, M.S. Ravenscroft, S. Punturi, Multiple electron tunneling paths across self-assembled monolayers of alkanethiols with attached ruthenium (II/III) redox centers, J Phys Chem. 100 (1996) 18852-18858. https://doi.org/10.1021/jp962831q

[37] F. Lisdat, and D. Schäfer, The use of electrochemical impedance spectroscopy for biosensing, Anal Bioanal Chem. 391 (2008) 1555. https://doi.org/10.1007/s00216-008-1970-7

[38] P. Agarwal, M.E. Orazem, L.H. Garcia Rubio, Measurement models for electrochemical impedance spectroscopy I. Demonstration of applicability, J Electrochem Soc. 139 (1992) 1917-1927. https://doi.org/10.1149/1.2069522

[39] J.M. Esteban, and M.E. Orazem, On the application of the Kramers Kronig relations to evaluate the consistency of electrochemical impedance data, J Electrochem Soc. 138 (1991) 67-76. https://doi.org/10.1149/1.2085580

[40] B.A. Boukamp, A Linear Kronig Kramers Transform Test for Immittance Data Validation, J Electrochem Soc 142 (1995) 1885-1894. https://doi.org/10.1149/1.2044210

[41] Z. Balevicius, J. Talbot, L. Tamosaitis, I. Plikusiene, A. Stirke, G. Mickiene, S. Balevicius, A. Paulauskas, A. Ramanavicius, Modelling of immunosensor response: the evaluation of binding kinetics between an immobilized receptor and structurally-different genetically engineered ligands, Sens Actuators B 297 (2019) 126770 https://doi.org/10.1016/j.snb.2019.126770

[42] 40 M-J. Chiu, L-Y. Fan, T-F. Chen, Y-F. Chen, J-J. Chieh and et al, Plasma tau levels in cognitively normal middle-aged and older adults, Front Aging Neurosci. 9 (2017) 51. https://doi.org/10.3389/fnagi.2017.00051

[43] M. Sjögren, H. Vanderstichele, H. Ågren, O. Zachrisson, M. Edsbagge, et al, Tau and Aβ42 in cerebrospinal fluid from healthy adults 21–93 years of age: establishment of reference values, Clin Chem. 47 (2001) 1776-1781. https://doi.org/10.1093/clinchem/47.10.1776

[44] B.R. Kumar, and T.S. Rao, AFM Studies on surface morphology, topography and texture of nanostructured zinc aluminum oxide thin films, Dig J Nanomater Biostruct. 7 (2012) 1881-1889.

[45] J.O. Esteves-Villanueva, H. Trzeciakiewicz, S. Martic, A protein-based electrochemical biosensor for detection of tau protein, a neurodegenerative disease biomarker, Analyst. 139 (2014) 2823-2831. https://doi.org/10.1039/c4an00204k

[46] 44 S.X. Wang, D. Acha, A.J. Shah, F. Hills, I. Roitt, et al, Detection of the tau protein in human serum by a sensitive four-electrode electrochemical biosensor, Biosens Bioelectron. 92 (2017) 482-488. https://doi.org/10.1016/j.bios.2016.10.077

[47] Y. Dai, A. Molazemhosseini, C.C. Liu, A single-use, in vitro biosensor for the detection of T-tau protein, a biomarker of neuro-degenerative disorders, in PBS and human serum using differential pulse voltammetry (DPV), Biosensors 7 (2017) 10. https://doi.org/10.3390/bios701001

[48] M. Ye, M. Jiang, J. Cheng, X. Li, Z. Liu and et al, Single-layer exfoliated reduced graphene oxide-antibody Tau sensor for detection in human serum, Sens Actuators B. 308 (2020). https://doi.org/10.1016/j.snb.2020.127692

[49] B. Shui, D. Tao, J. Cheng, Y. Mei, N.J. Renault, and Z. Guo, A novel electrochemical aptamer–antibody sandwich assay for the detection of tau-381 in human serum, Analyst. 143 (2018) 3549-3554. **https://doi.org/10.1039/C8AN00527C**

Tables

Table 1. Impedimetric parameters of neuro-biosensor design steps.

Neuro-biosensor	Rct (ohm)	C_{dl} (µF)	k^0 ($m.s^{-1}$)	K.K.T
ITO/rGO	350.5±1.9	1025± 41	2.3×10^{-6}	20.7
ITO/rGO/AuNP	308±2.2	16.4± 0.5	1.8×10^{-6}	3.1
ITO/rGO/AuNP/11-MUA	466.7±3.2	2.3±0.02	2.69×10^{-7}	9.3
ITO/rGO/AuNP/11-MUA/anti-Tau	529.7±3.6	2.3±0.02	2.12×10^{-7}	8.2
ITO/rGO/AuNP/11-MUA/anti-Tau/BSA	4460± 47.6	2.9± 0.03	--	0.5
1 pg/mLTau-441	5754± 52.6	2.8± 0.01	---	
20 pg/mL Tau-441	7145± 66.4	2.6± 0.03	--	
60 pg/mL Tau-441	8432± 68.2	2.6± 0.03	--	
100 pg/mL Tau-441	11080± 104.4	2.6± 0.03	--	
200 pg/mL Tau-441	12420± 133.4	2.6± 0.03	--	
300 pg/mL Tau-441	15920± 161.4	2.3± 0.02	--	
400 pg/mL Tau-441	17600± 175.4	1.8± 0.02	--	
500 pg/mL Tau-441	21640± 195	0.4± 0.004	--	

Table 2. Determination of Tau-441 concentrations in CSF and serum samples with the developed neurobiosensor system.

CSF number	Content of Tau-441 CSF ($pg.mL^{-1}$)	Addition content ($pg.mL^{-1}$)	Detection content ($pg.mL^{-1}$, n = 3)	RSD (%, n=3)	Recovery (%)
1	242	100	355.5 / 341.5 / 333.8	3.2	101.6
		400	695.5 / 633 / 648.8	4.9	102.6
2	188	100	302 / 295.5 /277.7	4.3	101.3
		400	566 /555.4 /572.6	1.5	96.1
3	303.5	100	414.5 /422.3 / 407.7	1.7	97.2
		400	705.5 / 717.7 / 726.6	1.5	102
4	395.7	100	501.1 / 492.5 / 523.3	3.1	102
		400	848 / 805.5 / 846.2	2.8	104.7
Serum number	Content of Tau-441 serum ($pg.mL^{-1}$)	Addition content ($pg.mL^{-1}$)	Detection content ($pg.mL^{-1}$, n=3)	RSD (%, n=3)	Recovery (%)
1	11.5	100	120 / 115.5 / 119.6	2.1	106.1
		400	419.5 / 433 / 408.8	2.6	102.2
2	22.7	100	125.5 / 133.3 /136	4.1	107.2
		400	425 /433.5 /420.6	1.5	100.9
3	10	100	115 /122.2 / 107.7	6.3	104.5
		400	417.7 / 407.9 / 415	1.2	101
4	15.9	100	122 / 132.5 / 123.3	4.5	108.6
		400	422 / 415.5 / 426.2	1.3	101.3
5	25.5	100	132.5 / 132.5 / 143.3	4.6	108.4
		400	425.5 / 435.5 / 436.9	1.4	101.7

Table 3. Comparison of the analytical properties of various Tau-441 biosensors reported in the literature.

Electrode configuration	Immobilization procedure	Measurement principle	Determination range	LOD	Ref.
Gold nanoparticle	tau-tau interaction	EIS	0.2 -1.0 µM	0.001 µm	[45]
Gold microband	Protein G layer	EIS and CV	0.0001 - 1000 pM	0.03 pM	[46]
Gold film	3-MPA SAMs	DPV	1000 pg/mL-10^4 pg/mL		[47]
GCE chemically exfoliated single-layer rGO	rGO grafted with anti-Tau antibody	SWV	0.08 pM-80 pM	75 fM	[48]
Gold electrode	aptamer–antibody sandwich assay	DPV	0.5 pM - 100 pM	0.42 pM	[49]
rGO-AuNP nanocomposite	11-MUA SAMs	EIS, CV and SFI	1-500 $pg.mL^{-1}$	0.091 $pg.mL^{-1}$	Present study

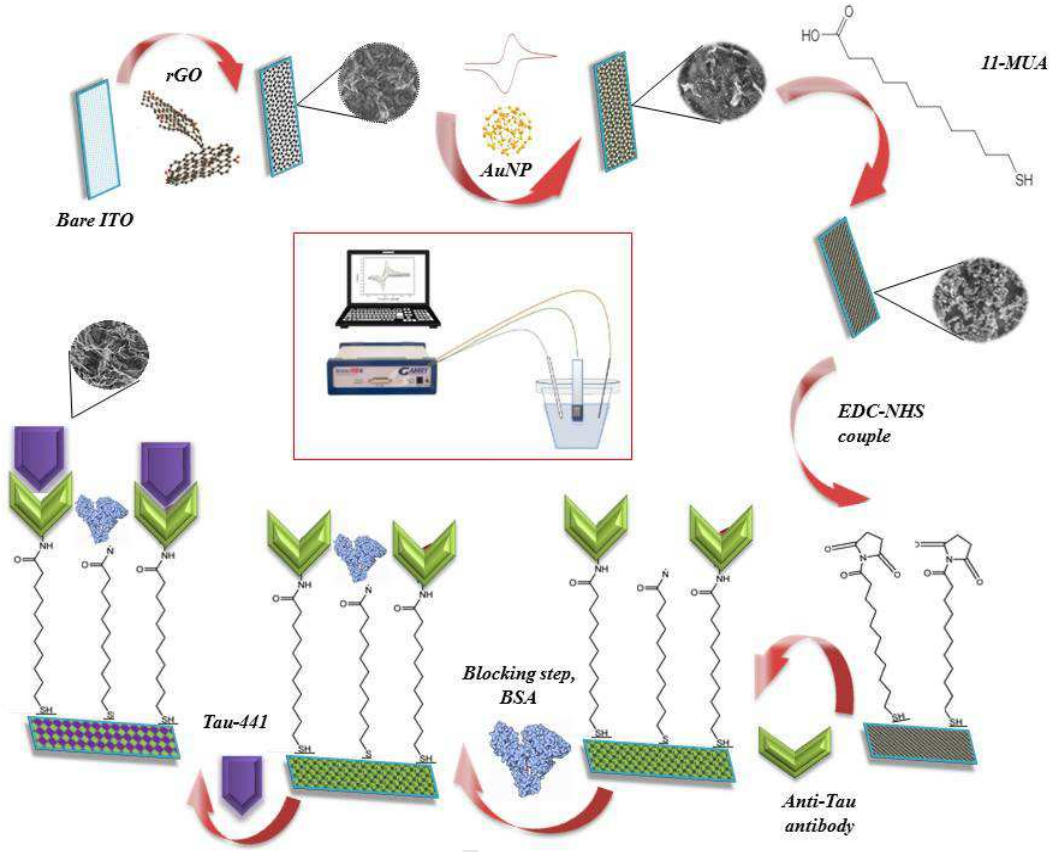

Scheme 1.

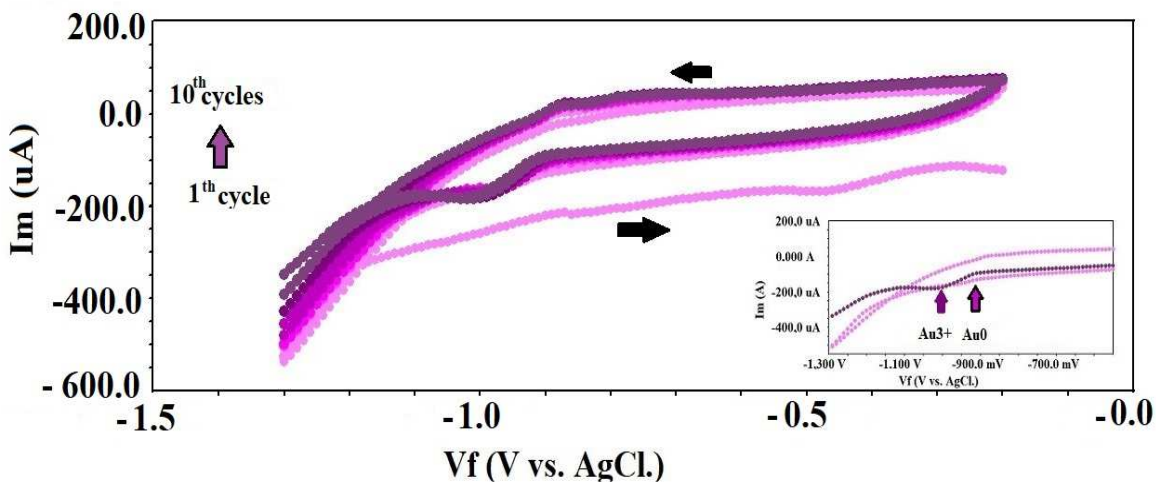

Figure 1.

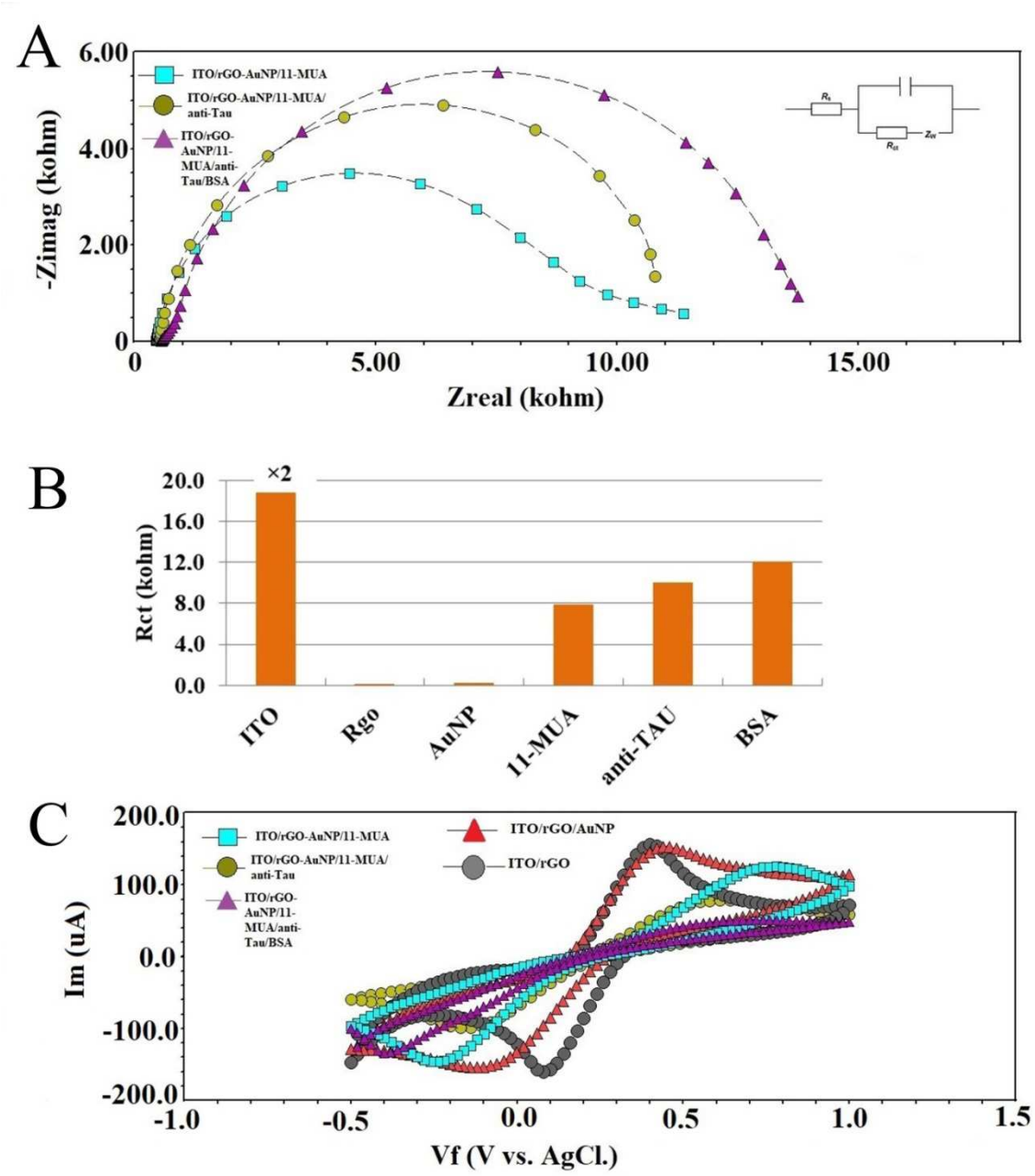
A
6.00
4.00
2.00
0
-Zimag (kohm)
0
5.00
10.00
15.00
Zreal (kohm)
ITO/rGO-AuNP/11-MUA
ITO/rGO-AuNP/11-MUA/ anti-Tau
ITO/rGO-AuNP/11-MUA/anti-Tau/BSA
B
×2
20.0
16.0
12.0
8.0
4.0
0.0
Rct (kohm)
ITO
Rgo
AuNP
11-MUA
anti-TAU
BSA
C
200.0
100.0
0.0
-100.0
-200.0
Im (uA)
-1.0
-0.5
0.0
0.5
1.0
1.5
Vf (V vs. AgCl.)
ITO/rGO-AuNP/11-MUA
ITO/rGO-AuNP/11-MUA/ anti-Tau
ITO/rGO-AuNP/11-MUA/anti-Tau/BSA
ITO/rGO/AuNP
ITO/rGO

Figure 2.

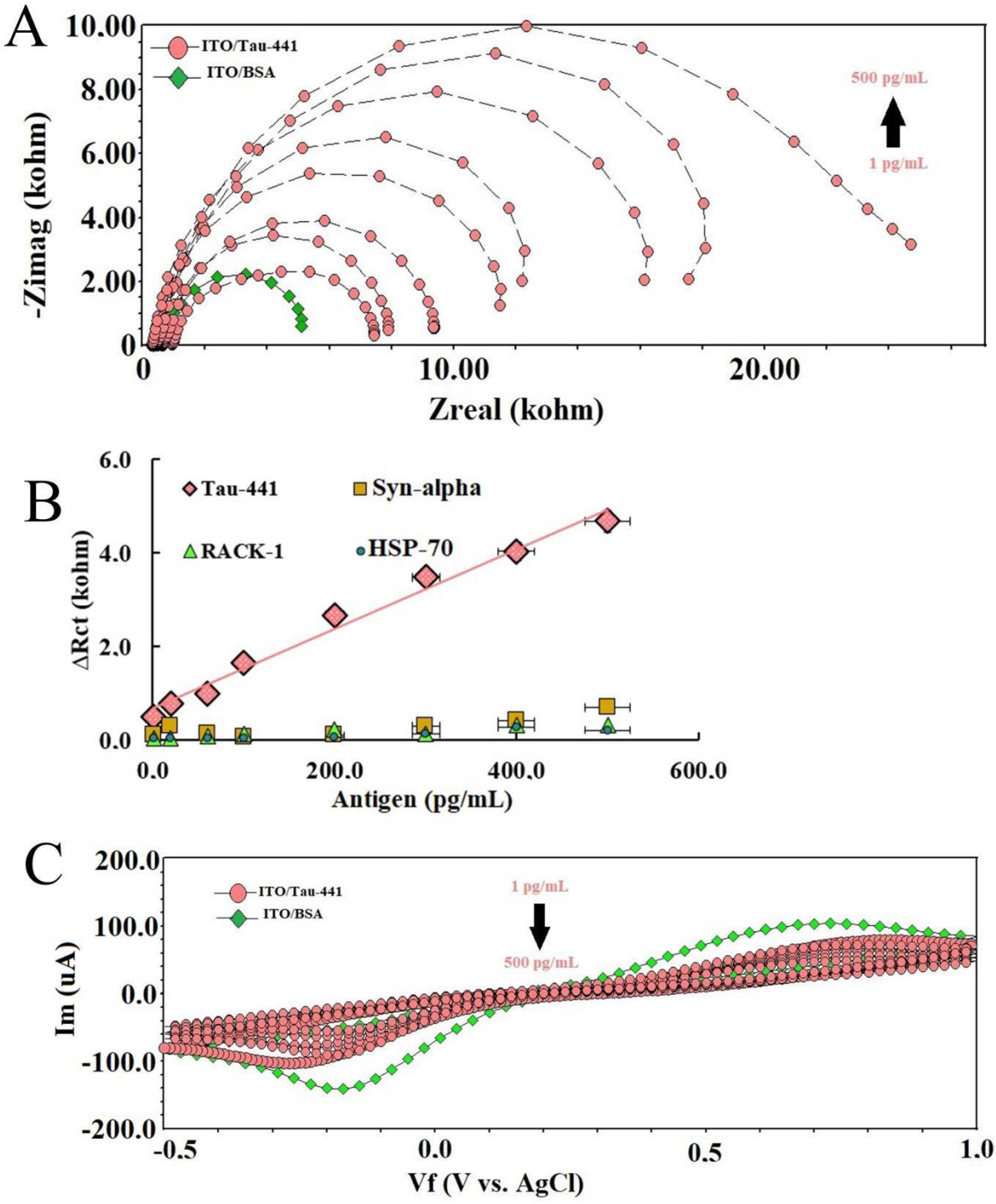
A
ITO/Tau-441
ITO/BSA
500 pg/mL
1 pg/mL
-Zimag (kohm)
Zreal (kohm)
B
Tau-441
Syn-alpha
RACK-1
HSP-70
ΔRct (kohm)
Antigen (pg/mL)
C
ITO/Tau-441
ITO/BSA
1 pg/mL
500 pg/mL
Im (uA)
Vf (V vs. AgCl)

Figure 3.

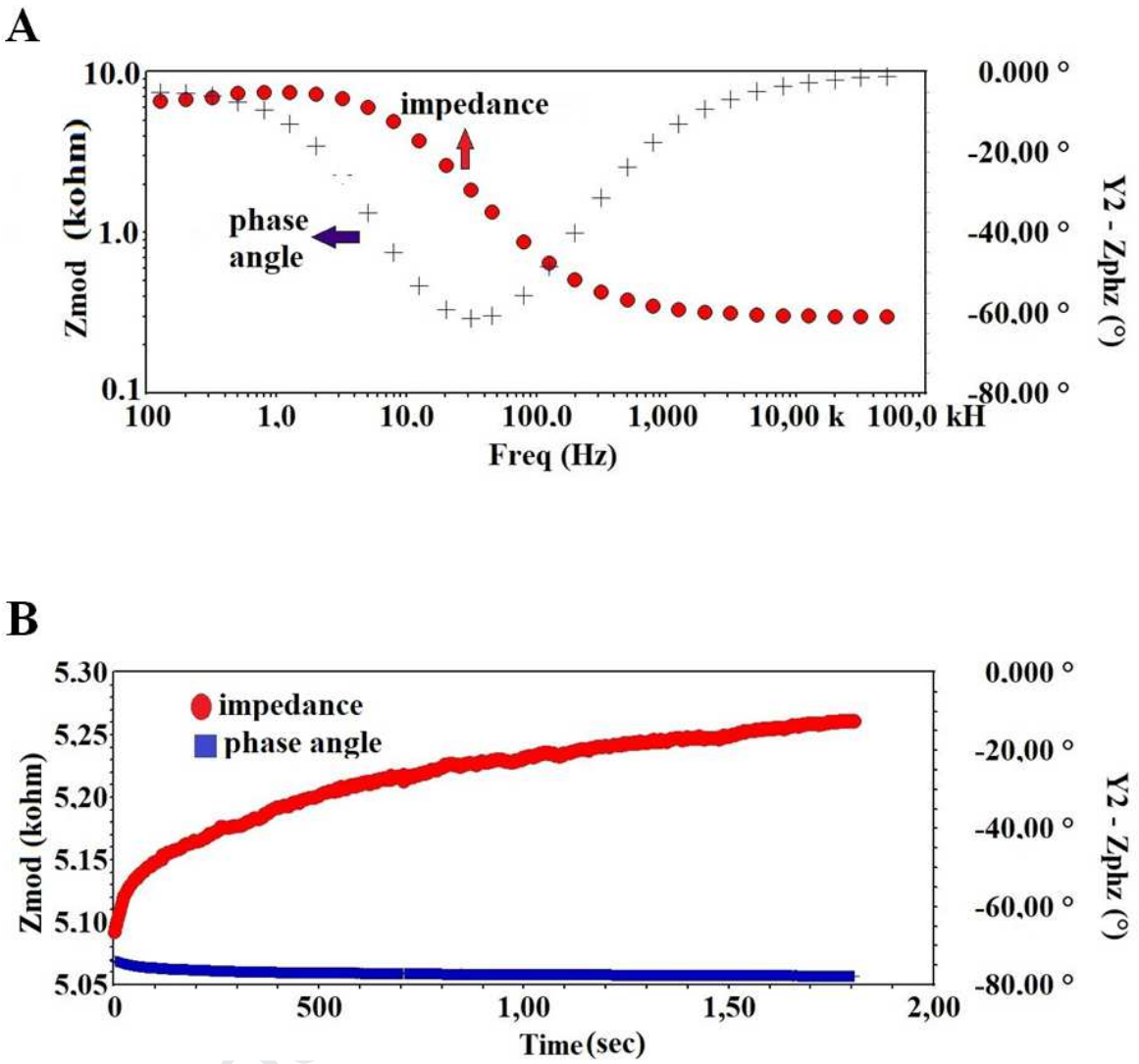
A
10.0
1.0
0.1
Zmod (kohm)
impedance
phase
angle
100
1,0
10.0
100.0
1,000
10,00 k
100,0 kH
Freq (Hz)
0.000 °
-20,00 °
-40,00 °
-60,00 °
-80,00 °
Y2 - Zphz (°)
B
5.30
5.25
5.20
5.15
5.10
5.05
Zmod (kohm)
impedance
phase angle
0
500
1,00
1,50
2,00
Time (sec)
0.000 °
-20,00 °
-40,00 °
-60,00 °
-80,00 °
Y2 - Zphz (°)

Figure 4.

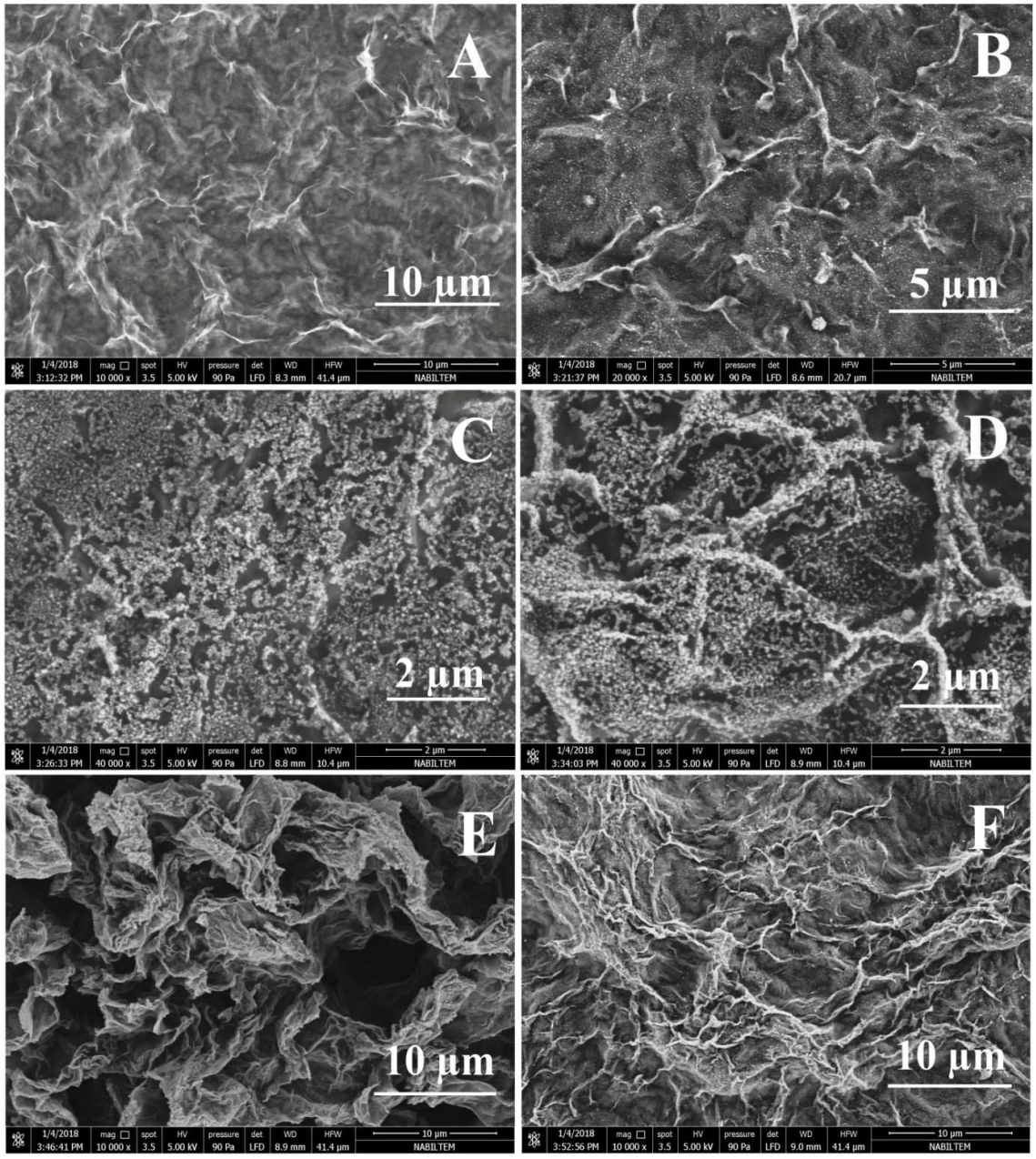
A
10 µm
1/4/2018 3:12:32 PM mag 10 000 x spot 3.5 HV 5.00 kV pressure 90 Pa det LFD WD 8.3 mm HFW 41.4 µm 10 µm NABILTEM
B
5 µm
1/4/2018 3:21:37 PM mag 20 000 x spot 3.5 HV 5.00 kV pressure 90 Pa det LFD WD 8.6 mm HFW 20.7 µm 5 µm NABILTEM
C
2 µm
1/4/2018 3:26:33 PM mag 40 000 x spot 3.5 HV 5.00 kV pressure 90 Pa det LFD WD 8.8 mm HFW 10.4 µm 2 µm NABILTEM
D
2 µm
1/4/2018 3:34:03 PM mag 40 000 x spot 3.5 HV 5.00 kV pressure 90 Pa det LFD WD 8.9 mm HFW 10.4 µm 2 µm NABILTEM
E
10 µm
1/4/2018 3:46:41 PM mag 10 000 x spot 3.5 HV 5.00 kV pressure 90 Pa det LFD WD 8.9 mm HFW 41.4 µm 10 µm NABILTEM
F
10 µm
1/4/2018 3:52:56 PM mag 10 000 x spot 3.5 HV 5.00 kV pressure 90 Pa det LFD WD 9.0 mm HFW 41.4 µm 10 µm NABILTEM

Figure 5.

Figure Legends

Scheme 1. Schematic presentations of immobilization steps for anti-Tau antibody.

Figure 1. Cyclic voltammograms of the gold nanoparticle depositing on the ITO electrode surface (Inserted subfigure shows the reduction peak of gold).

Figure 2. Electrochemical impedance spectra (A), charge transfer changes (B) and cyclic voltammograms (C) for immobilization steps. EIS (initial frequency: 50 000 Hz, final frequency: 0.05 Hz, points: 5, formal potential 0 V) and CV (potential between −500 mV and 1000 mV, scan rate: 100 mV s−1, step size: 10 mV).

Figure 3. Impedance spectra obtained for different concentrations of Tau-441 (A), concentration-dependent calibration plot for tau-441 obtained using the neuro-biosensor based on anti-Tau under optimal working conditions (B), and cyclic voltammograms (C) obtained for different concentrations of Tau-441

Figure 4. Bode plot (A) and SFI spectrum of the designed neuro-biosensor.

Figure 5. Step-by-step morphological SEM images for the designed biosensor. (A) ITO/rGO, (B) ITO/rGO/AuNP, (C) ITO/rGO/AuNP/11-MUA, (D) ITO/rGO/AuNP/11-MUA/Anti-Tau, (E) ITO/rGO/AuNP/11-MUA/Anti-Tau/BSA, (F) ITO/rGO/AuNP/11-MUA/Anti-Tau/BSA/Tau-441

Highlights

This neurobiosensor in combination with rGO-AuNP-MUA developed for the selective determination of Tau-441, a prominent biomarker for AD.

The developed neuro-biosensor offers a wide determination range (1-500 $pg.mL^{-1}$) for target protein Tau-441, both in CSF and in serum samples.

Surface coverage values, pinholes and Kramers Kronig data of modified sensing-surface were determined in detail.

Declaration of interests

☒ The authors declare that they have no known competing financial interests or personal relationships that could have appeared to influence the work reported in this paper.

☐The authors declare the following financial interests/personal relationships which may be considered as potential competing interests: